**Research Paper** https://doi.org/10.7733/jnfcwt.2021.19.3.307

# A Systematic Approach for Mechanical Integrity Evaluation on the Degraded Cladding Tube of Spent Nuclear Fuel Under Transportation Pinch Force

Seong-Ki Lee[1], Joon-Kyoo Park[1], and Jae-Hoon Kim[2,*]
[1]*KEPCO Nuclear Fuel, 242, Daedeok-daero 989beon-gil, Yuseong-gu, Daejeon 34057, Republic of Korea*
[2]*Chungnam National University, 99, Daehak-ro, Yuseong-gu, Daejeon 34134, Republic of Korea*

(Received July 13, 2021 / Revised July 30, 2021 / Approved August 9, 2021)

This study developed an analytical methodology for the mechanical integrity of spent nuclear fuel (SNF) cladding tubes under external pinch loads during transportation, with reference to the failure mode specified in the relevant guidelines. Special consideration was given to the degraded characteristics of SNF during dry storage, including oxide and hydride contents and orientations. The developed framework reflected a composite cladding model of elastic and plastic analysis approaches and correlation equations related to the mechanical parameters. The established models were employed for modeling the finite elements by coding their physical behaviors. A mechanical integrity evaluation of 14 × 14 PWR SNF was performed using this system. To ensure that the damage criteria met the applicable legal requirements, stress-strain analysis results were separated into elastic and plastic regions with the concept of strain energy, considering both normal and hypothetical accident conditions. Probabilistic procedures using Monte Carlo simulations and reliability evaluations were included. The evaluation results showed no probability of damage under the normal conditions, whereas there were small but considerably low probabilities under accident conditions. These results indicate that the proposed approach is a reliable predictor of SNF mechanical integrity.

Keywords: Spent nuclear fuel, Dry storage, Mechanical integrity, Transportation, Degradation, Probability

*Corresponding Author.
Jae-Hoon Kim, Chungnam National University, E-mail: kimjhoon@cnu.ac.kr, Tel: +82-42-821-6645

**ORCID**
Seong-Ki Lee http://orcid.org/0000-0001-8083-6227
Joon-Kyoo Park http://orcid.org/0000-0002-1426-2656
Jae-Hoon Kim http://orcid.org/0000-0001-9025-5401

## 1. Introduction

Spent Nuclear Fuel (SNF) is one of the most sensitive physical and chemical properties that are difficult to deal with and to define its characteristics. It is challenging to prove the mechanical integrity and ensure other safety-related elements required by law [1-3]. In addition, as the degree of burnup level increases, the material degradation escalates, which accelerates oxidation and hydrogen concentration of the fuel rod cladding acting as the front-line containment of radioactive materials in SNF regardless of its type. Especially during the dry storage, hydrogen and its hydride precipitation are concerned as the key material elements. From the perspective of mechanical integrity depending on the stress and temperature environment, this hydride is a weak element of cladding tube. The mechanical state of this precipitated hydride is relatively brittle compared to zirconium alloy, the parent of the cladding tube. Particularly, it sensitively responds to the dynamic load expected in SNF transportation and storage management environment. Although limited to specific material properties (phases), the elastic coefficient of hydride is about 12–25% and its hardness is about 40% of zircaloy base metal. And also, the fracture toughness is 50 to 100 times lower compared to the cladding mother material, which indicates that it is significantly weak and brittle properties [4]. The hydride contents and reorientation are considered as important issues to be identified and evaluated technically for the long-term dry storage of SNF. In particular, the IAEA expects that dry storage will be implemented in many major nuclear countries in America, Europe and Asia for a very long period even beyond hundreds of years [5]. To keep up with this trend and support it technically, various kinds of evaluation methodologies were developed. However, researches nowadays mainly focus on hydride production, hydride rearrangement mechanism and its local behavior in SNF cladding tube. Existing assessment approaches reflecting the comprehensive mechanical response characteristics of SNF are not detailed and systematic enough to be a general assessment approach. The US Department of Energy (DOE) was the first to conduct an extensive evaluation of SNF damage under transportation and handling for dry storage against lower degree of SNF burnup [6], but did not take material behavior considering this kind of hydride effects. Damage criteria such as fracture strain and toughness were also used in combination with deterministic and probabilistic treatments by establishing a correlation equation with insufficient database. As a follow-up study to the DOE's research, Electrical Research Institute (EPRI) also conducted a mechanical integrity evaluation by introducing a new evaluation criterion called strain energy (SE) covering hydride degradation effects for the higher degree of SNF burnup [7]. Although this methodology was relatively complete study, some evaluation items were omitted and to be improved, and the technical background connected with the mechanistic theory was lacking in some level. In this study, existing systems were introduced and benchmarked to make the physical model of SNF cladding system with commercial codes, ABAQUS, and the mechanical characteristics of cladding composite system with hydrides were sub-programmed and applied to this scheme. Various improvements have been also made to improve completeness of overall evaluation system. In modeling this methodology, the clad mixed with hydride was regarded as a composite material system, and was defined by linking the related theory and hydride directions when establishing preliminary constraints for mechanical modeling. Elastic and plastic regions were separated with the concept of SE to ensure the damage criteria meet the applicable legal requirements. These two damage criteria can be applicable for normal and hypothetical accident conditions, respectively. In addition, the thickness of cladding tube was modeled after subtracting the oxide film as thin as possible for a conservative evaluation when modeling the fuel rod geometry. Finally, by integrating all these works into the analytic system, the general mechanical evaluation system was completed reflecting SNF's degraded characteristics. Then, the verification was performed by comparing the results of the existing

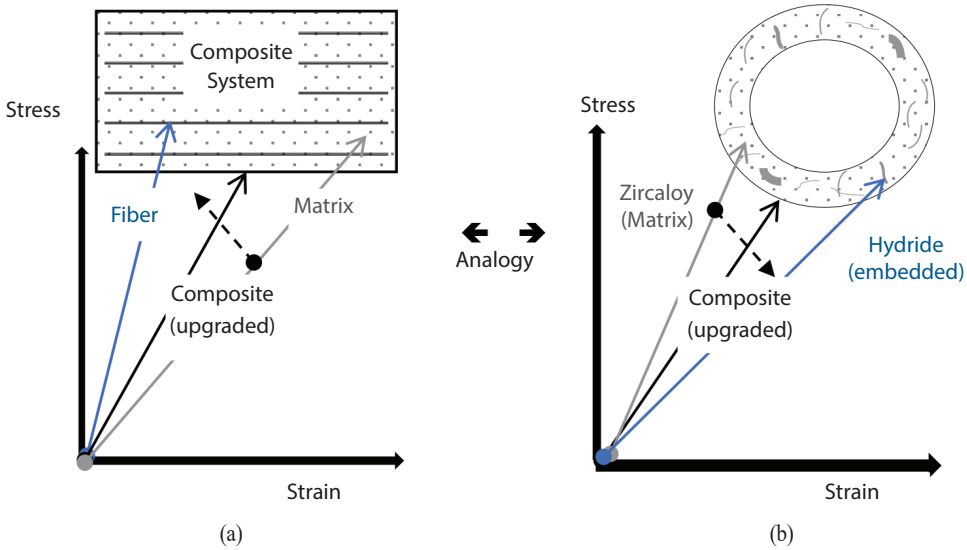


(a) (b)

Fig. 1. Analogy between general composite and SNF cladding tube with hydride embedded: (a) General composite; (b) SNF cladding tube with hydride embedded.

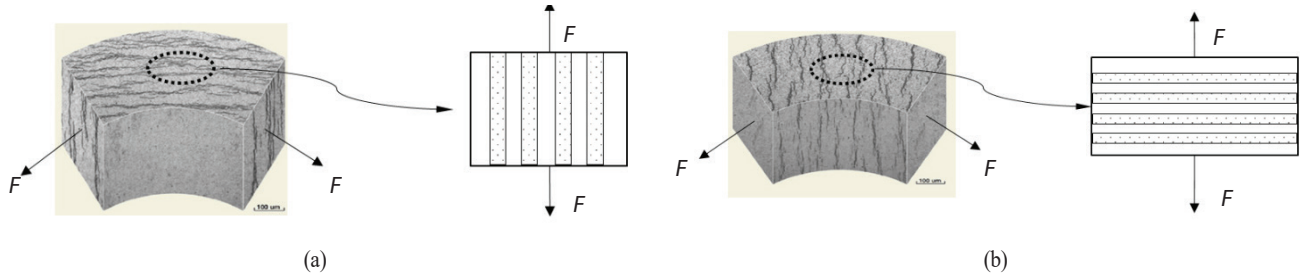


(a) (b)

Fig. 2. Circumferential and radial hydrides in cladding tube: (a) Iso-strain model; (b) Iso-stress model.

verified evaluation. Using this development system, the practical evaluation on 14 × 14 SNF was performed with a probabilistic reliability approach. The boundary conditions in the analysis considered the longitudinal pinch impact load that is the highest potential failure in reaction with the radial hydride under normal and hypothetical accident conditions. This approach can be applied to evaluate other loading modes such as cladding lateral damage mode.

## 2. Materials and Methods

### 2.1 Mechanical Characterization of Cladding Tube With Hydride

A new mechanical material characteristic model that reflects the effects of hydride ought to accurately evaluate cladding tube that are subject to normal and accidental conditions. In this study, the cladding is treated as a composite material composed of zirconium alloy matrix and the hydride platelets. These have separate material phases with their own elastoplastic and fracture properties. The interacting phenomena at their interfaces shall be simply defined with appropriate constraint conditions to ensure strain and stress compatibility. The developed model with the existing practices and the composite theory featured in multi-phase damage behavior which modeled the complex interaction between the hydride phases and the alloy matrix, and the coupled effect of radial and circumferential hydrides on

cladding stress-strain response. In this section, a more detailed process deals with the study of the similarity between the composite structure and hydride morphology, and the modeling approach related to the elastoplastic behavior.

### 2.1.1 Analogy Speculation Between Cladding Tube With the Hydride-embedded Composite

The first step is to set up an analogous composite system which has vertical and horizontal embedded matters in matrix to simulate the material state field of cladding tube with circumferential and radial hydride platelets. In the case of common composite materials, the material stiffness can be increased by inserting a reinforced fiber with high strength and rigidity for the purpose of artificially strengthening the parent metal [8]. Regarding to SNF cladding tubes, the mechanical properties of the alloy mother material are relatively better than those of hydrides that are naturally produced as an inferior one. Hydrides make a degraded mixture by operating environmental factors such as temperature, stress, hydrogen, and so on. Thus, SNF cladding tube can be defined as the opposite concept of degraded composite or mixture, in this case, it makes the material's equivalent toughness lower. Fig. 1 shows the conceptual plot of clad-to-composite analogous for stress-strain behavior of these two mixtures.

Hydrides in the cladding tube have circumferential or radial direction as shown in Fig. 2, but there are also hydrides distributed in random directions. This can be defined in extreme dichotomous way in the circumferential and radial directions to enhance the usefulness of the damage evaluation by applying the rule of mixtures. This methodology is to create an analytical framework that vertically responds to each action load, and simultaneously results in conservatism and simplification of the analysis. The direction of the hydride is defined in longitudinal and transverse directions to simplify the mixture (the base of the mixture) and the hydride (embedded material) as shown in Fig. 2. Fig. 2(a) shows a simplified simulation of circumferential hydride, and it can be assumed that the interfacial coupling between the cladding parent and hydride is considered very high. The deformation is same as in the longitudinal direction based on the same length. These systems are considered as iso-strain model and can be represented as follows:

$$\varepsilon_c = \varepsilon_m = \varepsilon_h \tag{1}$$

where $\varepsilon_m$ and $\varepsilon_h$ are the clad matrix and hydride strain respectively, then $\varepsilon_c$ is the composite mixture strain. In this model, the total load ($F_c$) of the mixture can be expressed by resultant stress corresponding to the matrix load ($F_m$) and the hydride load ($F_h$) respectively. Equation (2) represents each phase as an area fraction of the entire mixture and the equivalent volume fraction ($V$) if the length is the same as the following:

$$F_c = F_m + F_h \rightarrow \sigma_c = \frac{\sigma_m A_m}{A_c} + \frac{\sigma_h A_h}{A_c} = \sigma_m V_m + \sigma_h V_h \tag{2}$$

where the subscriptions $c$, $m$ and $h$ are the composite (clad/hydride), matrix (clad) and implanted hydride respectively. Assuming that each element of the mixture is elastic deformation, it can be expressed as an elastic modulus, $E$, using the condition of Equation (2) as follows:

$$\frac{\sigma_c}{\varepsilon_c} = \frac{\sigma_m}{\varepsilon_m} \cdot V_m + \frac{\sigma_h}{\varepsilon_h} \cdot V_h \rightarrow E_c = E_m V_m + E_h V_h = E_m (1 - V_h) + E_h V_h \tag{3}$$

where equation $V_h + V_m = 1$ is used. On the other hand, Fig. 2(b) can be regarded as an simplified model equivalent to radial hydride. This can be represented by an iso-stress model since it can be assumed that the sectional area could be same in each phase. So the model condition can be expressed as follows:

$$\sigma_c = \sigma_m = \sigma_h \tag{4}$$

Similar to the equivalent strain model, the strain equilibrium state can be expressed as follows:

$$\varepsilon_c = \varepsilon_m \cdot V_m + \varepsilon_h \cdot V_h \rightarrow \frac{\sigma_c}{E_c} = \frac{\sigma_m}{E_m} V_m + \frac{\sigma_h}{E_h} V_h \quad (5)$$

Rearranging the Equation (5), equivalent elastic modulus can be expressed as Equation (6).

$$E_c = \frac{E_m E_h}{E_m V_h + E_h V_m} = \frac{E_m E_h}{E_m V_h + E_h (1 - V_h)} \quad (6)$$

The equivalent elastic models of equations (3) and (6) are a series of linear combination of materials and a parallel combination of properties, respectively. These expressions indicate the upper and lower bounds of the theoretical equivalent elastic coefficients, respectively, depending on the function of volume fraction of each phase. This means the structural response characteristic may be a weaker property when stress is applied vertically to a hydride compared to the parallel one. The following equations are added to express the relation between overall stress and strain.

$$\varepsilon_{ij}^{c} = \varepsilon_{ij}^{c_1} \cdot V_m + \varepsilon_{ij}^{c_2} \cdot V_h \quad (7)$$

$$\sigma_{ij}^{c} = \sigma_{ij}^{c_1} \cdot V_m + \sigma_{ij}^{c_2} V_h \quad (8)$$

$C_1$ and $C_2$ stand for matrix and hydride platelet conditions (phases), and "$ij$" are local coordinate system basis axis i.e. $ij$ = 12, 23, 33 for Equation (7) and 11, 22, 12 for Equation (8) in Fig. 3, respectively. The overall stress-strain relations for each phase and mixture are represented by local and global coordinate systems, respectively, as follows:

$$\sigma_{ij}^{c_1} = D_{ijkl}^{EP(c_1)} \cdot \varepsilon_{kl}^{(c_1)},\ \sigma_{ij}^{(c_2)} = D_{ijkl}^{EP(c_2)} \cdot \varepsilon_{kl}^{(c_2)} \quad (9)$$

where $D^{EP}$ is elastoplastic constitutive tensor in each phase and $ijkl$, each index has 1, 2 and 3.

$$\sigma_{ij}^{C} = D_{ijkl}^{EP(C)} \cdot \varepsilon_{kl}^{(C)} \quad (10)$$

$D_{ijkl}^{EP(C)}$ derived for individual phases is a single material elasticity configuration matrix introduced from the standard elastoplastic scheme composed of equivalent elastic moduli in Equations (3) and (6). Equation (10), the global mixture reconstruction, is constructed by merging Equation (9) according to expressions (7) and (8) of the iterative computation process. Each phase is taken to J2-elastoplastic process, with an isotropic hardening material.

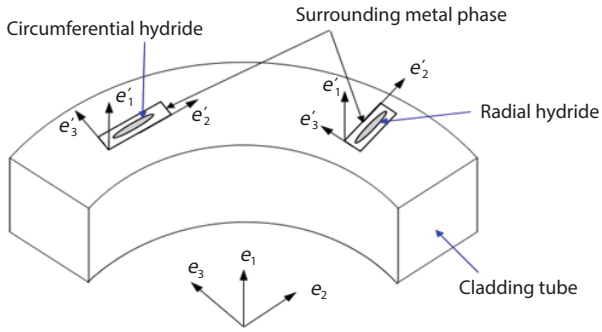


Fig. 3. Global and local coordinate system for the circumferential and radial hydride in the cladding tube.

The relation between the uniaxial stress-strains for each phase is shown below [9-11]:

$$Y = Y_0 \left\{ 1 + \left( \frac{\varepsilon}{\varepsilon_0} \right)^n \right\} \quad (11)$$

where $Y$ and $Y_0$ are the current and initial yield stresses respectively, and $\varepsilon$ is the equivalent plastic strain. $Y_0$, $\varepsilon_0$, and n are the material constants and determined independently for each phase. Stress calculations for each phase are performed using a radial-return method with the constraints in Equations (1) and (4) enforced iteratively at the constitutive level. These constraints are employed to define the construction equations considering the equivalent material system to obtain the load response characteristics. In addition, existing damage assessments performed with the focused combination of radial hydride-to-hoop stress induced by the pinch load may be reasonable [11]. However, in the case of circumferential hydride, there are no obvious differences from the perspective of the system strength as identified in equations (3) and (6). Thus, any systems of vertical direction loads to hydride shall be identified and evaluated generally unlike the existing evaluation approach. These

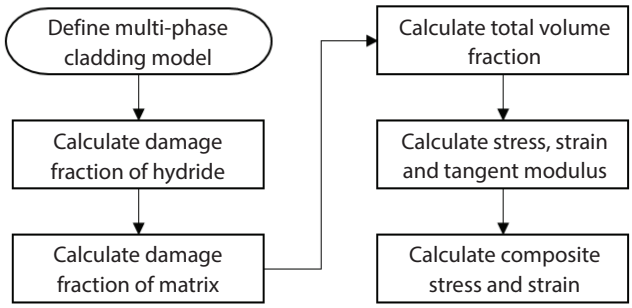


Fig. 4. Overall process of cladding strength analysis.

findings are to be used as the basic elements of composing the material constitution and failure evaluation approaches addressed in the following sections.

#### 2.1.2 Modeling Approach of Cladding Strength Analysis

The implementation of the elastoplastic constitutive relations in a finite element context requires the finite element discretization in the usual way [12, 13] with the equation system as follows:

$$\mathrm{K}\,\mathrm{u} = \mathrm{f} \tag{12}$$

where f is the applied force and K is the stiffness matrix given by

$$\mathrm{K} = \int_{\Omega} B^{T}\,\mathrm{D}_{ijkl}^{EP(C)}\,B\,d\Omega \tag{13}$$

where $B$ is the strain-displacement and $D^{EP}$is the elastoplastic constitutive matrix defined in Equations (9) and (10) respectively.

Multi-phase configuration model was established on a mixed theory of typical hydride features of high degree of burnup cladding tubes in Ref. [9, 10]. This can enable direct prediction of cladding damage by external forces, and add damage to each material considering the interaction between each phase so that material damage can be simulated in the model. Connecting this model with constitutive matrix in Equation (13), the described stress and strain relation of the cladding containing hydride, and the damage modification defined the calculation of the damage volume fraction of the composite containing hydride. Using the constitutive and damage models, the cladding tube strength analysis can be evaluated as overall process shown in Fig. 4.

### 2.2 Structural Integrity Evaluation Approach

The overall approaches for structural evaluation of cladding tube reflecting hydride characteristics were constructed as shown in Fig. 5, which was implemented by synthesizing the previous proven cases and theories. The first step is to define the cladding damage mode stated in the mechanical response analysis under the lateral drop event during the SNF transportation causing the pinch load between fuel rod-to-rod and fuel rod-to-space grids. The SNF cladding structural response can be classified into three potential damage modes depending on the drop events as shown in Fig. 6 [15]. Mode I damage can occur when the strain exceeds the material's ductility limit, but it does not mean it reaches failure. This destruction mode could occur under a variety of drop impact conditions (vertical, horizontal, edge, and inclined) and is most likely to occur under horizontal fall conditions as bending occurs dominantly in the supporting lattice areas in contact with the cladding during the impact. Mode II damage can be seen as an extension of Mode I's lateral crack fracture mode. A small lateral crack such as a hairline and pinhole shape in mode I caused a complete fracture of the entire section. Mode III damage is a load condition caused by contacting fuel rods and is the main route of longitudinal break. In particular, pinch loading occurs due to collisions of fuel rods and support grids, fuel rods and fuel rods, fuel rods and internal structures of transportation, which are dominant in horizontal and inclined fall conditions. This study mainly deals with the Mode III damage evaluation.

In order to assess the damage phenomena, the degradation conditions of the cladding after long-term dry storage

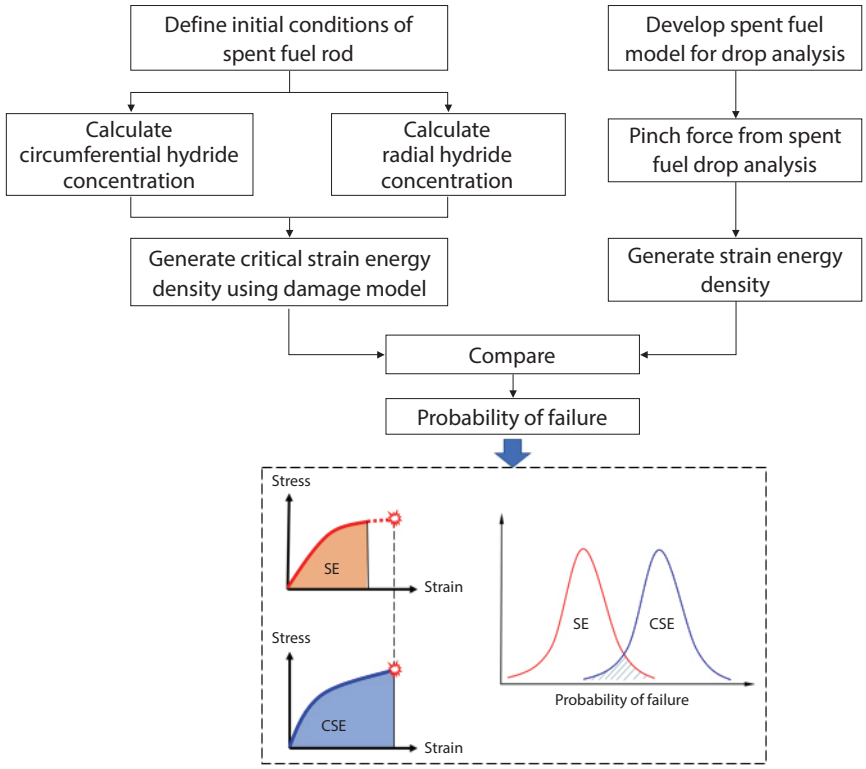


Fig. 5. Procedure for fuel rod longitudinal damage evaluation.

| Failure Modes during SNF tranportation/handling | Remarks |
|---|---|
| 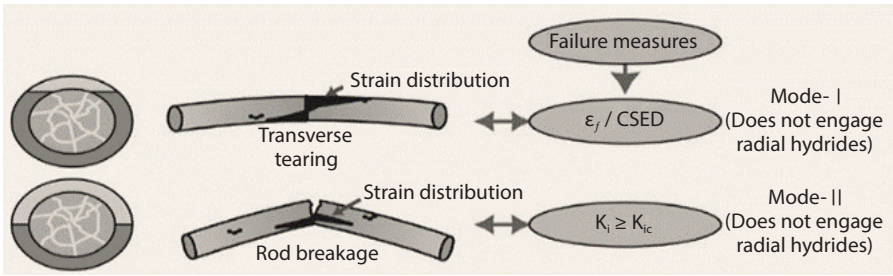 | Circumferential hydride concerned |
| 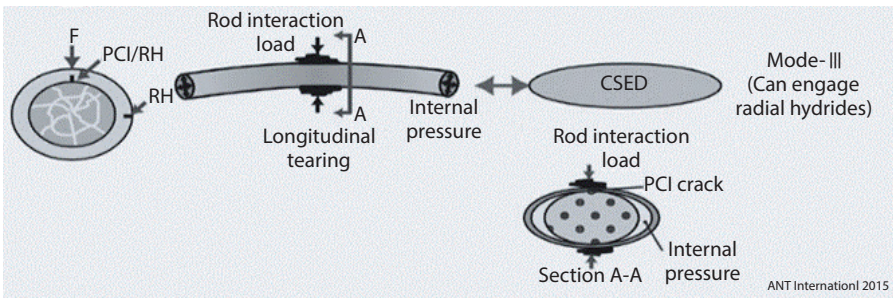 | Reoriented radial hydride concerned (Scope of this study) |



Fig. 6. Spent fuel rod failure modes under cask drop in horizontal orientation [15].

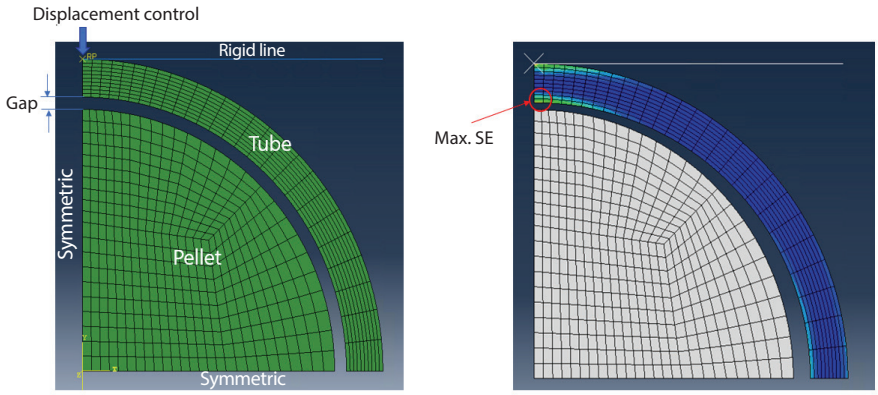


Fig. 7. FE model for longitudinal failure of cladding tube and maximum corresponding SE.

shall be considered conservatively. Especially, the rearrangement of hydride can reduce ductility and cause a longitudinal damage to the cladding due to the pinch load reacted with the radial hydride, which forms the iso-stress mode in Fig. 2. The strain energy density (SE) is used to evaluate the probability of break as an assessment measure. The reason for using the scalar parameter of the energy concept is to rationally define the mechanical properties depending on the hydride distribution. This is independent path unlike vector and tensor physical quantities such as stress and strain that are path-dependent with non-repeatability and with many uncertainties.

The concentration of hydrogen in circumferential direction is a by-product of oxide corrosion of cladding tube, and the radial hydride is determined by the pressure and temperature through reorientation mechanism in cladding tube. The critical strain energy density (CSE) can be calculated by using the defined circumferential and radial hydride concentrations and the mentioned models hereafter. The SE due to a drop event can be calculated by using the global model composed of a cask and SNFs [14] and the detailed fuel rod model that has elements of cladding, uranium pellet, and the gap between cladding and pellet having a significant effect on longitudinal damage. Once the probability distribution of the CSE and SE under impact loads is defined, the damage probability can be calculated using the probabilistic analysis and the reliability evaluation.

Table 1. SE and CSE analysis conditions for the definition of material properties

| Parameters | Values |
|---|---|
| Temperature [℃] | 181.58 (453.73 K) |
| Fast neutron fluence [n·m$^{-2}$] | $7.5 \times 10^{25}$ |
| Circumferential hydride concentration [ppm] | 0–2,000 (0 only for SE) |
| Radial hydride concentration [ppm] | 0–200 (0 only for SE) |

## 2.3 Finite Element Modeling of Hydrided Cladding Tube

The finite element (FE) model for the cladding integrity evaluation was developed by using the methodology of mechanical characteristic behavior in multi-phase cladding as mentioned in the previous section for 14 × 14 SNF with commercial FE program, ABAQUS. The FE model used in the analysis was a 1/4 fuel rod cross-sectional symmetry model, as shown in Fig. 7, and the cladding material property is defined [16] in Table 1 conditions. For conservative evaluation of material properties, a specific temperature condition was applied to reflect a long-term dry storage degradation over 40 years by the cladding tube. The cladding-to-pellet clearance was set very small to simulate the end-of-life conditions of the nuclear fuel. The SE was calculated due to the change in a pinch load of mode III and

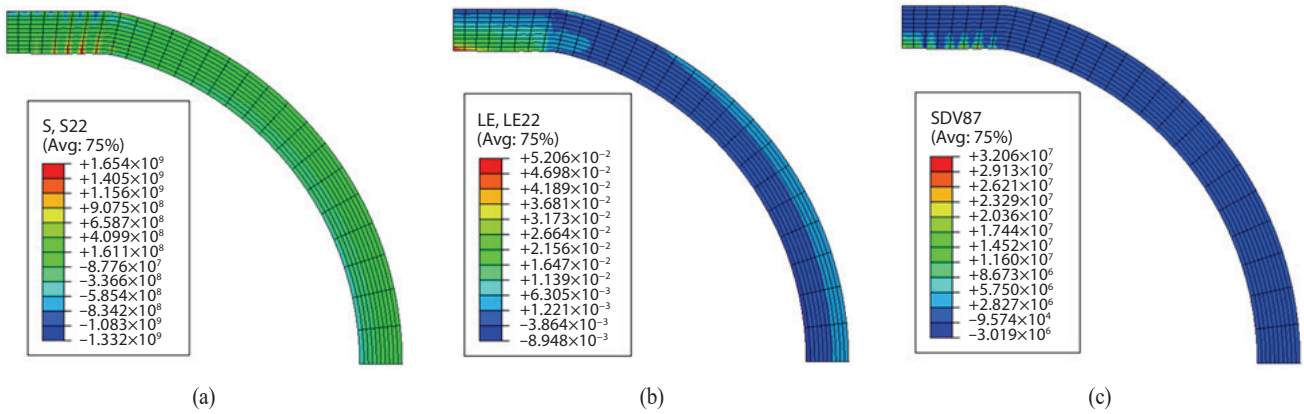


(a) (b) (c)

Fig. 8. SE analysis results for 70 $\mu$m gap: (a) Hoop stress [Pa]; (b) Hoop strain [m·m$^{-1}$]; (c) SE [Pa].

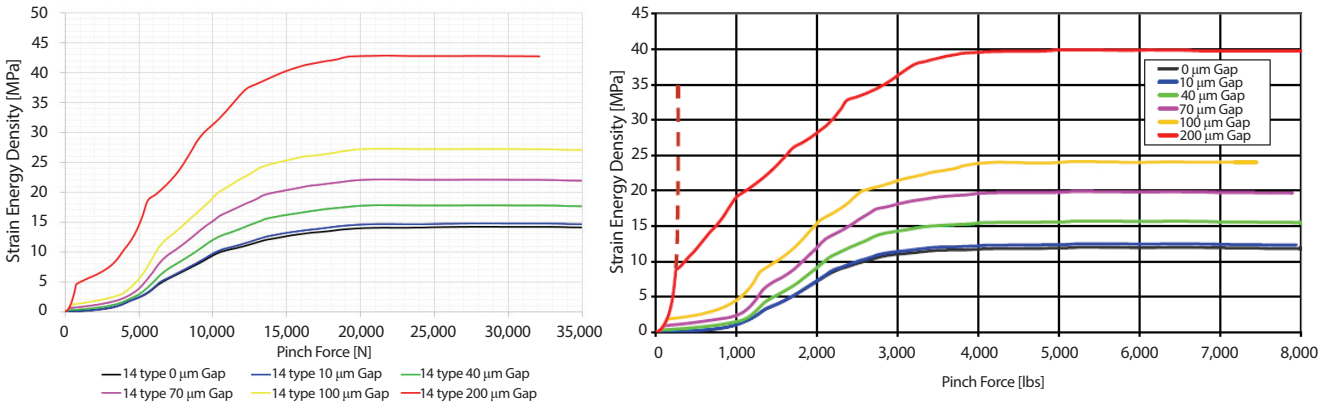


(a) (b)

Fig. 9. Pinch force as function of imposed displacement: (a) 14 × 14 SNF modeling results; (b) 17 × 17 SNF EPRI [11].

cladding-to-pellet gap ranged from 0 $\mu$m to 200 $\mu$m. In order to calculate the SE according to the pinch load, at first, a rigid line was applied to the upper surface of the cladding tube for compulsory displacement in the direction of compression, and the reaction force was checked corresponding to the displacement.

The SE can be calculated depending on the specific concentrations of circumferential and radial hydrides, but hydrogen-free conditions were applied to generate a maximum SE for conservative evaluation. The SE was calculated based on the tensile stress and strain in the circumference of the cladding tube, as the following equation:

$$SE = \int_0^{\varepsilon_\theta} \sigma_\theta \, d\varepsilon_\theta \quad for\ \sigma_\theta \geq 0 \text{ (only tension)} \qquad (14)$$

where $\sigma_\theta$, $\varepsilon_\theta$ are the hoop stress and strain respectively in the cladding tube.

The SE can be calculated by using the stress and strain of each element integration point. Fig. 7 shows that the maximum SE caused by the upper cladding tube deformation is generated from the inside of the element. The maximum SE was selected for conservative evaluation among nine integration points of SE values. Fig. 8 shows the hoop stress, hoop strain, and SE distribution of the cladding tube of top surface at a displacement of 0.000375 meter when the cladding-to-pellet gap was 70 $\mu$m, indicating that the maximum SE occurred inside the cladding tube. Here, only the SE considered the tensile load component in the hoop direction, which affected cladding damage to the radial

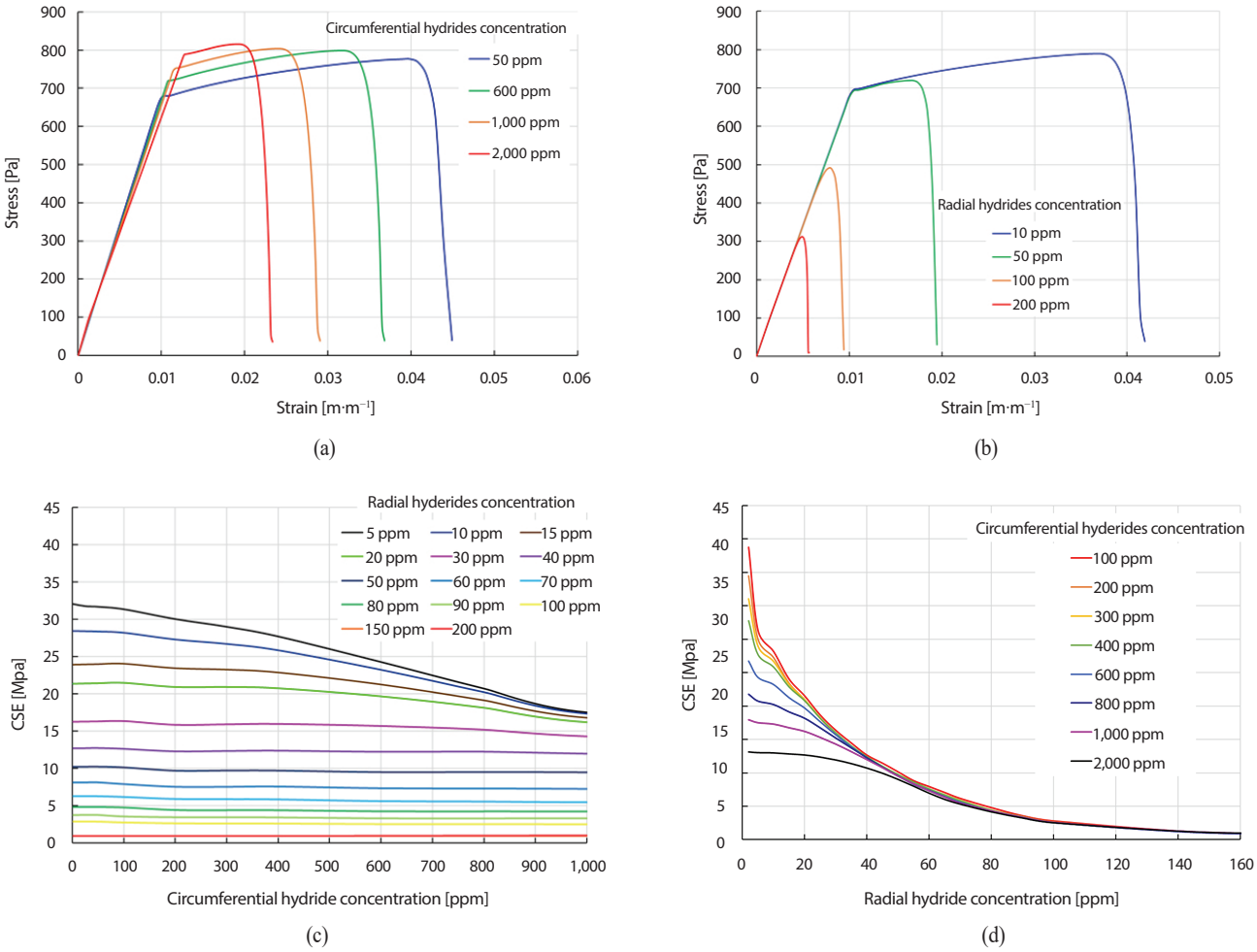


Fig. 10. Stress-strain and CSE response for various hydride conditions: (a) Stress-strain curve for various circumferential hydride at 10 ppm of radial hydride; (b) Stress-strain curve for various radial hydride at 300 ppm of circumferential hydride; (c) CSE-circumferential hydrides for various radial hydrides; (d) CSE-radial hydrides for various circumferential hydrides.

hydride vertically. The hoop stress at 12 o'clock direction inside the cladding tube was caused by the tensile force while the external stress was due to the compression. Fig. 9 shows the maximum SE with increasing pinch load, indicating that the SE under all gap clearance conditions increased the load to 20,000 N and remained almost constant. The calculation results were compared to EPRI's result [11] for verification of the model indirectly. Although the comparison was with different types of SNFs, almost similar values and trends are shown when the unit conversion is considered. This calculated SE is to be used as a basis for determining longitudinal and penetrating damage to the cladding with hydrides hereafter.

Another FE model was developed to calculate CSE as a structural integrity criterion. The model used axial symmetry tubes and was applied with the same material properties with the SE analysis. To consider the irradiation effect of the cladding, the neutron fluence in the end-of-life conditions was employed, and the hydride concentration was varied under the assumption that the distribution was uniform in the thickness direction as mentioned in Table 1. The displacement was applied to the inner wall of the tube

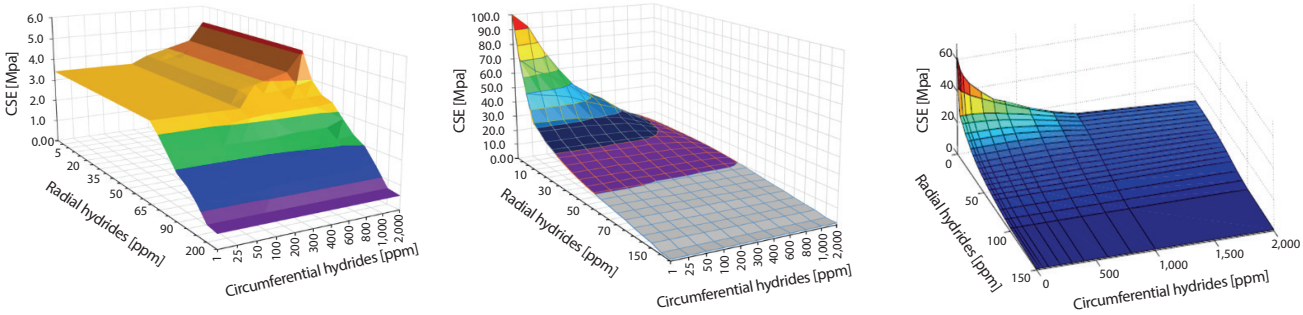


Fig. 11. CSE as functions of circumferential and radial hydride concentrations: (a) 14 × 14 SNF CSE for elastic; (b) 14 × 14 SNF CSE for elastic and plastic; (c) 17 × 17 SNF CSE EPRI [11].

model. The Zircaloy and hydride hardening behavior was defined using the MATPRO [16]. The stress-strain fields and their CSE response are shown in Fig. 10. According to the variation of hydride conditions, the yield stress increased slightly as the concentration of its augments, but the CSE decreased noticeably. The increased concentration of hydride was to reduce the ductility of the cladding. It was found that the concentration of a radial hydride had a greater effect on the CSE than the circumferential one as shown in Figs. 10(c) and 10(d). This is the phenomenon in line with the maximum and minimum equivalent mechanical properties of the composite in iso-stress and strain conditions as previously mentioned. This, in theory, proved the reason why a radial hydride shall be considered and a dominant factor for under the longitudinal failure mode of the cladding behavior. In other words, a high concentration of radial hydride led to a sharp decrease in CSE and was not affected by circular hydride at a high concentration of radial hydride.

Fig. 11 is a three-dimensional surface plot of the CSE according to the radial and circumferential concentrations for elastic and plastic regions, this can be expressed as below equation:

$$U_{CSE} = U^e + U^p = \int_0^{\varepsilon^{el}} \sigma_{ij}\, d\varepsilon_{ij} + \int_{\varepsilon^{el}}^{\varepsilon^{el}+\varepsilon^p} \sigma_{ij}\, d\varepsilon_{ij} \qquad (15)$$

where $U_{CSE}$, $U^e$ and $U^p$ are total, elastic and plastic CSEs, respectively.

Unlike the previous approaches [6, 11], this intends to perform an integrity evaluation separately under the normal and hypothetical accident conditions specified in relevant laws and regulations. Two CSEs were determined by each fraction of circumferential and radial hydride. The CSE decreased as the radial hydride concentration increased. The CSE in the elastic region, there is a little change for the same circumferential hydride when the radial hydride is less than 60 ppm because the CSE in the plastic region changes greater than that in the elastic region. That was, at 60 ppm and above, only the elastic region of CSE existed, and the elastic region of CSE decreased as the hydride increased. And also, it was confirmed that the CSE decreased as the hydride increased, reducing the resistance capacity due to load, especially the effect of the radial hydride. The total trend of CSE showed similar results as the previous analysis [11] as shown in this figure even though the CSE values were slightly different due to dissimilarity in fuel design feature and reactor irradiation conditions.

## 2.4 Probabilistic Integrity and Damage Evaluation

Probabilistic and reliability evaluation methodologies were introduced to consider the scatterability of the damage contributors such as an external load, oxide thickness,

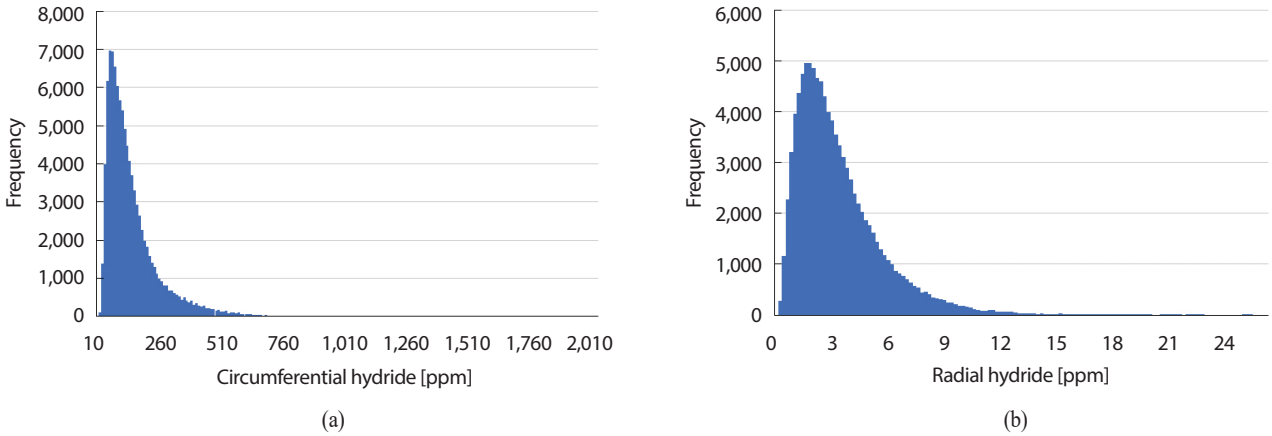


Fig. 12. Probability distributions of hydride concentrations for 14 × 14 SNF cladding tube: (a) Circumferential hydride concentration; (b) Radial hydride concentration.

hydride contents, etc., and to draw a reasonable evaluation.

At first, we calculated the probability density distributions of SE and CSE of 14 × 14 fuel rods using Monte Carlo Simulation (MCS) methodology with the commercial program EXCEL and its Visual Basic function under normal and accident drop modes during the SNF transportation conditions to evaluate the fuel rod longitudinal damage probability under normal and hypothetical accident conditions respectively. For the implementation of MCS, a random number generation function in EXCEL and reliable probability distributions of the examination and test data such as internal pressure, oxide thickness, and temperature of cladding tube were used. As shown in Fig. 5, in order to generate a probability distribution of CSE, the circumferential and radial hydride concentrations must be calculated using the initial conditions of the SNF fuel rods. The circumferential hydride concentration is determined by the hydrogen contents due to corrosion of the cladding tube [11]. The radial hydride concentration is determined by the hoop stress which depends on the internal pressure and the dry storage temperature history of the fuel rod [17]. The radial hydride concentration was calculated using the hydride reorientation model in reference 17. Unlike laboratory test results under conservative and artificially simulated temperature and stress conditions, the calculations were executed with a practical model assuming that the hoop stress decreases due to decay heat for more than 40 years. The CSE was calculated using the defined circumferential and radial hydride concentrations and Fig. 11. Fig. 12 shows the probability distributions of the hydride concentrations generated using MCS by applying the initial conditions of 14 × 14 SNF fuel rods in dry storage. Although the concentration of radial hydride is very small compared to that of circumferential hydride, as shown in Fig. 10(d), a small amount of radial concentration affects the CSE on a small scale and this should be considered in the evaluation.

The SE due to the impact force can be calculated using the pinch force from the SNF drop analysis, the pellet-cladding gap and Fig. 9. The pellet-cladding gap is calculated by considering the creep that depends on the history of the cladding temperature and internal pressure. Fig. 13 shows the probability distributions of pellet-cladding gap and pinch force under normal and hypothetical accident conditions form drop analysis.

Next, the damage probability was evaluated by applying a reliability assessment method with the stress-strength model, which was defined as follows [18]:

$$\begin{aligned} R &= \int_0^\infty f_{SE}(r) \cdot [1 - F_{CSE}(r)]\, dr \\ &= 1 - \int_0^\infty f_{SE}(r) \cdot F_{CSE}(r)\, dr \\ &= 1 - P_f \end{aligned} \tag{16}$$

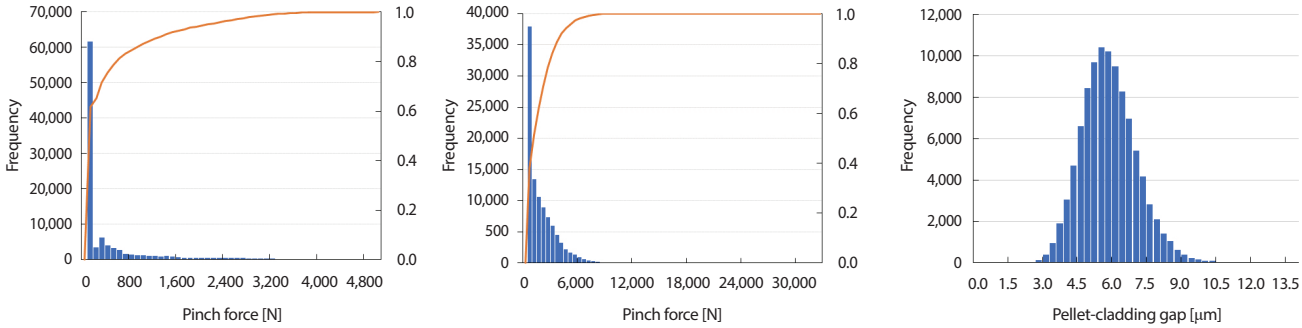


(a) (b) (c)

Fig. 13. Probability distributions of pinch forces and pellet-cladding gap for 14 × 14 SNF: (a) Pinch force 0.3-m-drop normal condition; (b) Pinch force 9-m-drop accident condition; (c) Pellet-cladding gap.

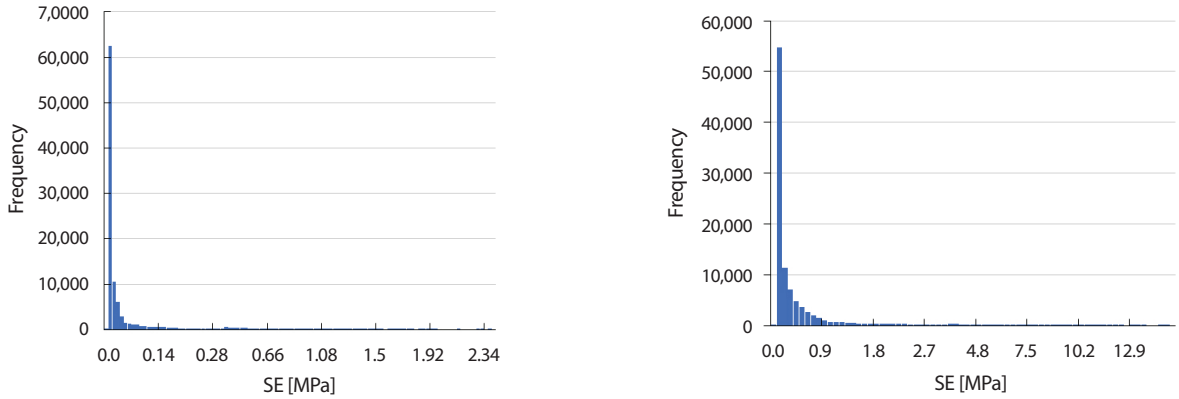


(a) (b)

Fig. 14. Probability distributions of SE for 14 × 14 SNF: (a) 0.3-m-drop normal condition; (b) 9-m-drop accident condition.

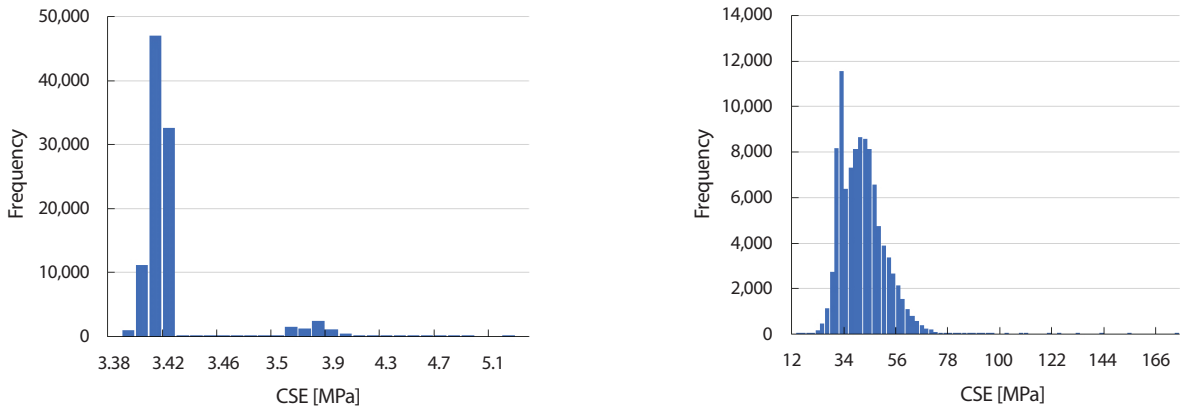


(a) (b)

Fig. 15. Probability distributions of CSE for 14 × 14 SNF: (a) 0.3-m-drop normal condition; (b) 9-m-drop accident condition.

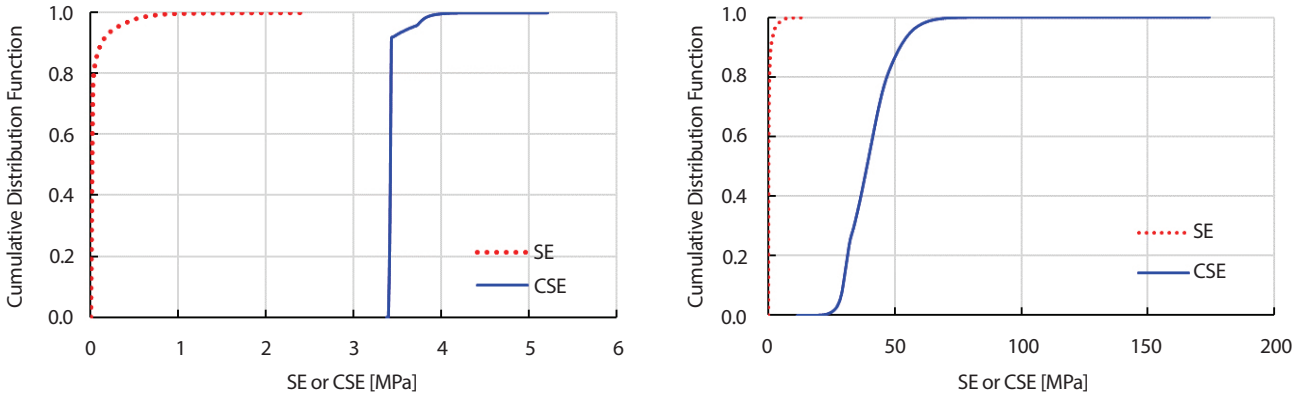


Fig. 16. Cumulative distribution functions of SE and CSE for 14 × 14 SNF: (a) 0.3-m-drop normal condition; (b) 9-m-drop accident condition.

Table 2. Longitudinal failure probability of 14 × 14 spent fuel rod under transportation

| Conditions | Failure probability (Failure type) | Existing evaluation | |
|---|---|---|---|
| | | DOE [6]* | EPRI [11, 19]** |
| Normal (0.3 m drop) | 0.0 | $3.0 \times 10^{-8}$ | Null |
| Accident (9 m drop) | $1.2 \times 10^{-9}$ (Partial failure) | $2.0 \times 10^{-5}$ | $1.0 \times 10^{-5}$ |

(* B&W 15 × 15 PWR fuel, **17 × 17 PWR fuel)

where $P_f$ denotes the failure probability. $f$ and $F$ are probability density function (PDF) and cumulative density function (CDF) for SE and CSE, respectively.

## 3. Results and Discussion

To calculate a failure reliability, CDF terms of Equation (16) must be calculated using the PDFs for each SE and CSE. Fig. 14 shows the probability distribution of SE using the fuel rod FE analysis in Fig. 9, the pinch force and gap information in Fig. 13. Fig. 15 shows the probability distribution of CSE using the hydride information of Fig. 12, and the relation between hydrides and CSE in Fig. 11.

Fig. 16 shows the calculated CDF for SE and CSE under normal (0.3-m drop) and accident conditions (9.0-m drop) respectively. Under the normal condition, Fig. 16(a) represents that the minimum CSE is greater than the maximum SE meaning that no damage has occurred. On the other hand, Fig. 16(b) shows the behavior of 9-m drop accident condition. This configuration is similar to the normal conditions. The integral of Equation (16) is approximated with trapezoidal rule by dividing SE values into sub-intervals. The final calculated damage probability $P_f$ is $1.2 \times 10^{-9}$. Table 2 summarizes evaluation results including the previous evaluation results of DOE and EPRI. As shown in the table, EPRI did not perform the evaluation with statistical methodology but in a rather deterministic way as a simple load comparison method under the normal condition [19]. In addition, the reason that this accident condition result is smaller than the existing ones is mainly caused by the smaller weight and design differences of 14 × 14 SNF compared the referenced SNFs 15 × 15 and 17 × 17 array, which have

the effect of reducing the drop impact energy. In conclusion, the evaluation results demonstrated in this paper are deemed reasonable.

## 4. Conclusions

In this study, a series of evaluation methodologies has been developed systematically by analyzing the existing approach and synthesizing various items affecting the cladding mechanical behavior as a mixture composite with embedded hydrides. The evaluation scheme of defined mechanical characteristics was employed in commercial FE modeling through a process of making codes with the user-defined subprogram. The composite of elastic and plastic theories, correlation equations related to a various of mechanical behavior parameters were incorporated into these general approaches. The model verification was also conducted by comparing the previous evaluation results. This developed model was applied to the 14 × 14 commercial SNF rods. In order for the damage criteria to meet the applicable regal requirements, the analysis results were separated into elastic and plastic areas with the energy concept parameters, i.e. CSE and SE and those were set up as damage criteria which can be applicable to normal and accident conditions, respectively, whereas the existing practice was not performed with normal condition. The probabilistic analysis results were used with Monte Carlo simulation and the reliability assessment theory for the longitudinal load mode that affects damage through interaction with radial hydrides during SNF transportation. The result of this work for 14 × 14 commercial SNF showed that there is no damage probability under normal conditions. DOE's evaluation result was also very close to zero-damage probability under the same condition. Regarding the accident condition, however, the result was $1.2 \times 10^{-9}$. This evaluation result of accident condition is small enough to be ignored. Therefore, it is reasonable to accept that the proposed approaches be practically and reliably to predict behavior and response of SNF cladding tube integrity reflecting dry-storage degradation effects.

## Acknowledgments

This work was supported by the Korea Institute of Energy Technology Evaluation and Planning (KETEP) grant funded by the Korea government (MOTIE) (20181710201770, Development of Evaluation Technology for Vibration and Shock Load Characteristics and PWR Spent Nuclear Fuel Integrity under Normal Conditions of Road and Sea Transport).

## REFERENCES

[1] International Atomic Energy Agency. Storage of Spent Nuclear Fuel, IAEA Report, Safety Standard Series No. SSG-15 (2012).

[2] United States Nuclear Regulatory Commission. Packing and Transportation of Radioactive Material, US NRC Report, 10 CFR Part 71 (2010).

[3] United States Nuclear Regulatory Commission. Licensing Requirements for the Independent Storage of Spent Nuclear Fuel, High-Level Radioactive Waste, and Reactor-related Greater Than Class C Waste, US NRC Report, 10 CFR Part 72 (2020).

[4] A. Strasser, R. Adamson, and F. Garzarolli. The Effect of Hydrogen on Zirconium Alloy Properties, ANT International Report, Volume I (2008).

[5] International Atomic Energy Agency. Selection of Away-From-Reactor Facilities for Spent Fuel Storage, IAEA Technical Report, IAEA-TECDOC-1558 (2007).

[6] T.L. Sanders, K.D. Seager, Y.R. Rashid, P.R. Barrett, A.P. Malinauskas, R.E. Eingziger, H. Jordan, T.A. Duffey, S.H. Sutherland, and P.C. Reardon. A Method for Determining the Spent-Fuel Contribution to Transport Cask Containment Requirements, US Sandia National

Laboraty Technical Report, SAND90-2406 (1992).

[7] A. Machiels. Dry Storage of High-Burnup Spent Fuel: Responses to Nuclear Regulatory Commission Requests for Additional Information and Clarification, Electric Power Research Institute Technical Report, 1009276 (2003).

[8] D.K. Lee et al, Composite Materials, Hongreung Science Publishing, Seoul (2007).

[9] J. Rashid, M. Rashid, and R. Dunham. Failure Criteria for Zircaloy Cladding Using a Damage-based Metal/Hydride Mixture Model, Electric Power Research Institute Technical Report, 1009693 (2004).

[10] J. Rashid, R. Dunham, M. Rashid, and A. Machiels, "A New Material Constitutive Model for Predicting Cladding Failure", Proc. of the Water Reactor Fuel Performance Meeting – WRFP/Top Fuel 2009, 127-129, September 6-10, 2009, Paris.

[11] J. Rashid, B. Dunham, Y. Zhang, and R. Montgomery. Spent Fuel Transportation Application: Longitudinal Tearing Resulting From Transportation Accidents – A Probabilistic Treatment, Electric Power Research Institute Technical Report, 1013448 (2006).

[12] O.C. Zienkiewicz, S. Valliappan, and I.P. King, "Elasto-plastic Solutions of Engineering Problems 'Initial Stress', Finite Element Approach", International Journal for Numerical Methods on Engineering, 1(1), 75-100 (1969).

[13] O.C.Zienkiewicz and R.L.Taylor, The Finite Element Method-Volume 2: Solid Mechanics, 5th ed., Hutterworth-Heinemann, Oxford (2000).

[14] Y. Yoo, K. Kim, K. Eom, and S. Lee, "Finite Element Analysis of the Mechanical Behavior of a Nuclear Fuel Assembly Spacer Grid", Nucl. Eng. Des., 352, 110179 (2019).

[15] C. Patterson and F. Garzarolli. Dry Storage Handbook-Fuel Performance in Dry Storage, ANT Internationl, Sweden (2015).

[16] L.J. Siefken, E.W. Coryell, E.A. Harvego, and J.K. Hohorst. SCDAP/RELAP5/MOD3.3 Code Manual: MATPRO- A Library of Materials Properties for Light-Water-Reactor Accident Analysis, US Nuclear Regulatory Commission Report, NUREG/CR-6150, Vol. 4, Rev. 2 (2001).

[17] J. Rashid and A. Machiels, "Hydride Precipitation in Spent Fuel Cladding During Storage", The 10th International Conference on Environmental Remediation and Radioactive Waste Management, September 4-8, 2005, Glasgow.

[18] K.C. Kapur and L.R. Lamberson, Reliability in Engineering Design, John Wiley & Son, New York (1977).

[19] J. Rashid, F. Wong, and R. Dunham. Spent Fuel Transportaion Application: Normal Conditions of Transport, Electric Power Research Institute Technical Report, 1015049 (2007).